JOURNAL OF EXPERIMENTAL AND THEORETICAL PHYSICS, 2024, Vol. 166, No. 2(8), pp. 230–238

ORDER, DISORDER AND PHASE TRANSITIONS IN CONDENSED MEDIA

MAGNETIC AND SUPERCONDUCTING PROPERTIES OF Fe-DOPED HIGH-TEMPERATURE SUPERCONDUCTORS YBaCuO SYNTHESIZED BY SOL-GEL METHOD

© 2024 K. S. Pigalskiy[a*], A. A. Vishnyov[a], N. N. Efimov[b], P. N. Vasiliev[b], A. V. Shabatin[c], L. I. Trakhtenberg[a, d]

[a]Semenov Federal Research Center for Chemical Physics of the Russian Academy of Sciences 119991, Moscow, Russia
[b]Kurnakov Institute of General and Inorganic Chemistry of the Russian Academy of Sciences 119991, Moscow, Russia
[c]Frumkin Institute of Physical Chemistry and Electrochemistry of the Russian Academy of Sciences 119071, Moscow, Russia
[d]Lomonosov Moscow State University 119991, Moscow, Russia
*e-mail: pigalskiy@gmail.com

Received February 28, 2024
Revised March 14, 2024
Accepted March 14, 2024

Abstract. For a series of iron-doped polycrystalline high-temperature superconductors $Y_{1-x}Fe_xBa_2Cu_3O_y$ ($0 \leqslant x \leqslant 0.05$), synthesized using the nitrate-citrate variant of the sol-gel method, studies of structural (by X-ray and electron microscopy methods) and magnetic (in alternating and constant magnetic fields) properties were conducted. For these samples, the dependencies of crystallographic parameters, crystallite sizes, superconducting transition temperatures on the doping level were determined, as well as the type and magnitude of magnetization hysteresis in fields up to 6 T. Field dependencies of intracrystalline critical current density *Jc* were calculated. It was shown that uniform distribution of the dopant throughout the crystallite volume due to the application of the sol-gel method leads to significant improvement in functional parameters compared to samples obtained by solid-state method. The microstructure improves, which is manifested in increased sizes and more distinct crystallite faceting, as well as narrowing of the temperature interval of transition to the superconducting state, increase in the magnitude of magnetic field hysteresis of magnetization and critical current. As a result, in sol-gel samples with iron doping level $x \approx 0.03$, an increase effect *Jc* exceeding an order of magnitude is achieved.

DOI: 10.31857/S004445102408e108

1. INTRODUCTION

Various methods of modifying the composition of ceramic materials through substitutions in cation sublattices are widely used to improve their functional characteristics. Examples include solid solutions based on rare-earth hafnates with increased ionic conductivity [1, 2], high-entropy multicomponent compositions of ferro- and piezoelectrics [3–5], rare-earth doping of materials for laser technology [6]. Cation substitutions also significantly influence the properties of high-temperature superconductors (HTSC). Interest in this topic is connected both with fundamental questions on the influence of defects on superconducting state parameters with *d*-wave symmetry of the superconducting order parameter [7, 8], and from an applied perspective. As known, local structure distortions created by doping are additional pinning centers and increase the density of intracrystalline critical current (J_c) [9]. For HTSC $YBa_2Cu_3O_y$ (YBaCuO) the effect on the value of *Jc* partial copper substitution in the chain plane by a number of elements was studied in [10–12], with the greatest effect of increase J_c (approximately 4-fold) obtained with substitution by Fe, Ga, and Mo. Another type of defect that increases J_c approximately twofold is the substitution of Ba with Sr in amounts of 1–5% [13].

A special place in this series belongs to the yttrium sublattice, as it allows not only partial but also complete substitution of Y with most rare-earth elements, which does not significantly affect the superconducting transition temperature (T_c) and other parameters of the superconductor [14, 15]. In particular, the resulting pinning does not lead to a noticeable increase in critical current. However, the effect of significant

increase *Jc* was recently discovered with another type of substitution in the yttrium position for a series of HTSC samples $Y_{1-x}Fe_xBa_2Cu_3O$ ($0 \leqslant x \leqslant 0.05$). For iron-doped HTSC YBaCuO, synthesized by the solid-state method, it was shown that the most effective is a small amount of doping near $x = 0.03$, at which the increase J_c in an external magnetic field of 1 T reaches an order of magnitude.

In samples with cation doping, an important characteristic is the degree of uniformity in the distribution of impurity atoms throughout the sample volume. In the case of the widely used solid-state method, multiple grinding of the sample between annealings is carried out to achieve uniformity. However, there are several other, more effective methods for synthesizing samples with a high degree of cation ordering, which are based on the stage of transferring initial cations into solution. One of them is the sol-gel process, which allows creating a uniform distribution of cations in the gel, and after its combustion, obtaining a batch consisting of a homogeneous mixture of nanosized particles of initial components [17]. Regarding HTSC YBaCuO, the main development of sol-gel methodology was aimed at synthesizing samples with small particle size. A nitrate-citrate variant of the sol-gel process was proposed and tested [18], which was later used in other works [19–21].

In this work, the influence of the uniformity degree of Fe bulk distribution on the properties of HTSC $Y_{1-x}Fe_xBa_2Cu_3O_y$, doped with iron in the range ($0 \leqslant x \leqslant 0.05$) was studied. Using sol-gel methodology at the initial synthesis stage, samples with a high degree of uniformity were obtained, their structural, magnetic and superconducting characteristics were determined and compared with corresponding characteristics of samples obtained by solid-state method.

2. EXPERIMENT

The first synthesis stage of each composition in the HTSC sample series $Y_{1-x}Fe_xBa_2Cu_3O_y$ (YFeBaCuO) ($x = 0$, 0.02, 0,03, 0,05) was the nitrate-citrate variant of the sol-gel process, allowing to obtain highly homogeneous nanosized batch. Compared to earlier works, the batch production technology was modified to improve its properties. While in works [17–19] the pre-dried gel (at 80°C) was burned in a muffle furnace during heating to 520°C, in this work the gel evaporation continued until its self-ignition. Afterward, the remaining soot was burned out of the obtained batch at $T = 600$°C (2 days).

Further synthesis of samples from sol-gel charge was carried out in an oxygen atmosphere in several stages. In the first stage, as a result of annealing at $T = 895$°C (48 h) in powder form and at $T = 925$°C (24 h) in compressed form, the reaction of forming the final compound YFeBaCuO proceeded almost completely. Then the samples were slowly heated (rate 1°C/h) to $T = 955$°C, during which intensive grain growth occurred, and the density increased to 93% of X-ray density. Oxygen saturation of the samples was carried out by slow cooling in oxygen flow from 920 to 380°C followed by holding for 20 h. The total oxygen content in all samples, determined by iodometric titration method, was $y \approx 6.92 \pm 0.03$.

A reference series of samples of the same compositions was obtained by solid-state method. To achieve phase equilibrium, the stoichiometric mixture of components Y_2O_3, Fe_2O_3, $BaCO_3$ and CuO was annealed in several stages in oxygen atmosphere with intermediate mechanical grinding. The temperatures and annealing times used in the synthesis of the studied samples are given in [16].

X-ray data were obtained using a Rigaku Smartlab SE diffractometer (K_α-radiation Cu) in the angle range $10° \leqslant 2\Theta \leqslant 120°$ with an interval of 0.01°. Structural parameters were calculated using the FullProf software package within the Pmmm space group.

The microstructure of the samples was studied using a QUANTA 650 FEG scanning electron microscope with field emission cathode. Series of microphotographs of various sections on the polycrystal cleavage were taken, followed by their quantitative analysis. Each crystallite on the cleavage surface (with total number of several hundreds) was assigned a circle diameter D, having an area equal to the visible area of the crystallite. Then a histogram of the distribution of values D was constructed, parameters of corresponding normal p_n and logarithmic normal p_{ln} distribution functions, average crystallite size D_{ev} and dispersion were calculated.

The transition temperature to the superconducting state was determined from measurements of temperature dependencies of low-frequency complex magnetic susceptibility (alternating magnetic field frequency 980 Hz, amplitude $h = 0.11$, 1.0 and 3.0 Oe).

Magnetization hysteresis measurements in an external field up to 6 T were performed using a PPMS-9 (Quantum Design) system. From the hysteresis magnitude, ΔM using the Bean critical state model formula for a cylindrical superconductor [22], the intracrystalline critical current density J_c was calculated:

$$J_c = 30\,\Delta M / D_{eff}. \quad (1)$$

This formula is valid in magnetic fields approximately twice exceeding the first magnetization maximum field, where one can assume $|M| \ll H \approx B$. The effective crystallite size D_{eff} included in formula (1), which determines the magnetization hysteresis magnitude of the polycrystal, does not coincide with the average size and is determined by the expression

$$D_{eff} = \int D^3 p_{ln}(D) dD \left[\int D^2 p_{ln}(D) dD \right]^{-1}. \quad (2)$$

When deriving (2), it was taken into account that the contribution to the magnetic moment of the sample from a superconductor with diameter D is proportional to $J_c D^3$, therefore the main contribution comes from the largest crystallites.

3. RESULTS AND DISCUSSION

An important criterion for choosing the synthesis method of doped HTSC YBaCuO was the possibility of achieving a high degree of uniformity in the distribution of impurity atoms throughout the sample volume. Fig. 1 (curve 2) shows a fragment of the diffraction pattern of sol-gel batch with sufficiently high content of Fe ($x = 0.08$), which demonstrates the absence of reflections from any iron compounds, including oxide. Furthermore, this diffraction pattern is completely identical to the diffraction pattern of the batch without iron (Fig. 1, curve 1). For comparison, Fig. 1 also shows the diffraction pattern of a stoichiometric mixture of commercial reagents Y_2O_3, Fe_2O_3, $BaCO_3$ and CuO corresponding to the composition with $x = 0.05$ (curve 3), where the peak from iron oxide is clearly visible. Thus, in the sol-gel batch, unlike the main components Y_2O_3, $BaCO_3$ and CuO, Fe_2O_3 did not crystallize, and iron is present in X-ray amorphous forms.

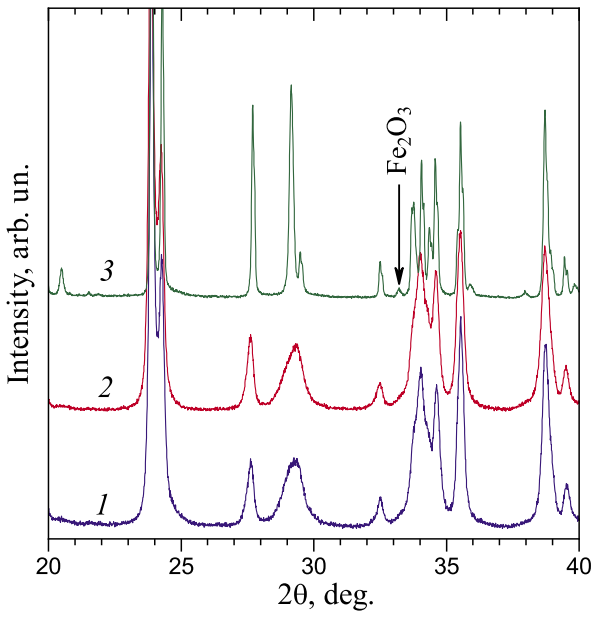

Fig. 1. X-ray diffractograms of sol-gel batches for synthesis of samples with composition $YBa_2Cu_3O_y$ (1), composition $Y_{0.92}Fe_{0.08}Ba_2Cu_3O_y$ (2). For comparison, a diffractogram of commercial reagents mixture Y_2O_3, CuO, $BaCO_3$, Fe_2O_3 in ratio corresponding to composition $Y_{0.95}Fe_{0.05}Ba_2Cu_3O_y$ (3) is shown. Arrow indicates the peak from Fe_2O_3

As a result of high-temperature annealing, samples of both series, obtained using both sol-gel process and solid-state method, had an orthorhombic structure. At the same time, Fe-containing samples showed a small amount of impurity phase $BaCuO_2$ (Fig. 2). With the increase of x, broadening and diffraction peak shift. Crystal lattice parameters and weight amount of impurity phase (Fract.), calculated using FullProf program within the P*mmm* space group, are given in the table. When changing the iron content, the lattice parameters of samples from both series change, the nature of these changes is similar to those obtained previously for structurally disordered samples without doping [23]. The most noticeable are the increase in parameter a and unit cell volume V_{cell}, as well as decrease in orthorhombic distortion $\sigma = (a - b)/(a + b)$, while the influence of synthesis method is weak. The presence of monotonic changes in lattice parameters with changing x confirms that Fe enters the HTSC structure.

The synthesis method manifested in clear differences in sample microstructures. Figs. 3*a, b* shows micrographs for samples SG3 and SR3 with iron content $x = 0.03$. Reducing the number of annealing cycles and intermediate grindings when using sol-gel batch allows for larger and well-formed crystallites, with these samples reaching 93% of X-ray density. The crystallite size dispersion proves to be quite large, and as Fig. 3*c* demonstrates, for sample SG3 the size range is from 10 to 65 μm. This figure also shows the corresponding distribution functions, with the logarithmic normal function providing the best agreement with experiment. The average crystallite sizes D_{ev} for all samples, calculated based on distribution function parameters, are shown in Fig. 3*d*. It is evident that due to the application of sol-gel methodology, the increase D_{ev} is from two to three times depending on x.

The values of T_c, determined from measurements of low-frequency magnetic susceptibility temperature dependencies, appear to be weakly dependent on the synthesis method (see Fig. 4 and Table). The content of iron $x \leqslant 0.03$ does not affect the value of T_c, a small decrease in T_c occurs at $x = 0.05$. At $x = 0.05$ there

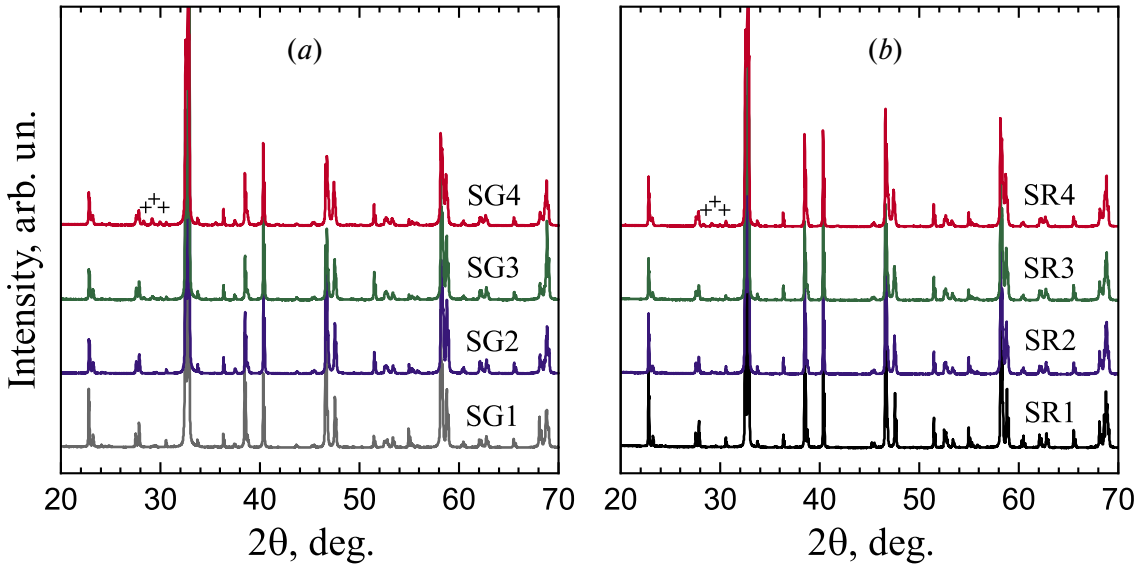

Fig. 2. X-ray patterns of HTSC samples $Y_{1-x}Fe_xBa_2Cu_3O_y$, synthesized using sol-gel process (*a*), solid-state method (*b*). Sample designations are shown near the curves. Crosses indicate peaks from impurity phase $BaCuO_2$

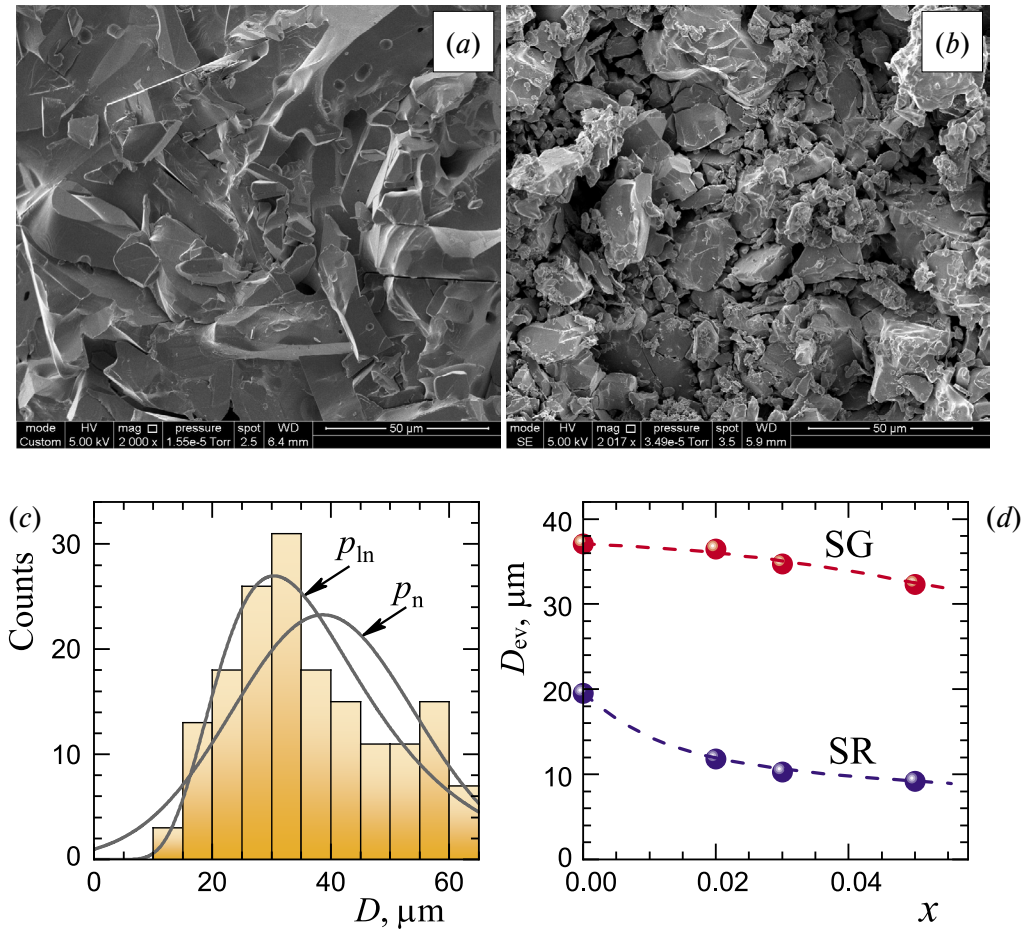

Fig. 3. Microphotographs of HTSC samples $Y_{0.97}Fe_{0.03}Ba_2Cu_3O_y$, synthesized using sol-gel process (*a*), solid-state method (*b*) (samples SG3 and SR3 respectively). (*c*) – Crystallite size distribution for sample SG3. Solid curves - corresponding distribution functions: normal (p_n) and lognormal (p_{ln}). (*d*) – Average crystallite size depending on iron content *x*. Sample series designations are shown near the curves

Table. Characteristics of the studied samples $Y_{1-x}Fe_xBa_2Cu_3O_y$, synthesized by sol-gel method (SG) and solid-state method (SR) with different iron content x: unit cell parameters a, b, c; unit cell volume V_{cell}; degree of orthorhombic distortion $\sigma = (b - a)/(b + a)$; amount of impurity phase $BaCuO_2$ (Fract.), temperature of superconducting transition onset T_c

Sample	x	a, Å	b, Å	c, Å	V_{cell}, Å^3	$10^3\sigma$	Fract.,wt%	T_c,K
SG1	0	3.8220	3.8875	11.688	173.66	8.5	0	91.6
SG2	0.02	3.8226	3.8840	11.681	173.43	8.0	0.06(1)	91.5
SG3	0.03	3.8244	3.8838	11.681	173.50	7.7	0.15(2)	91.4
SG4	0.05	3.8308	3.8820	11.683	173.74	6.6	4.02(5)	90.9
SR1	0	3.8196	3.8850	11.685	173.40	8.5	0	91.7
SR2	0.02	3.8242	3.8836	11.685	173.52	7.7	0.74(6)	91.7
SR3	0.03	3.8259	3.8825	11.684	173.55	7.3	0.82(8)	91.6
SR4	0.05	3.8317	3.8802	11.684	173.71	6.3	1.46(6)	91.3

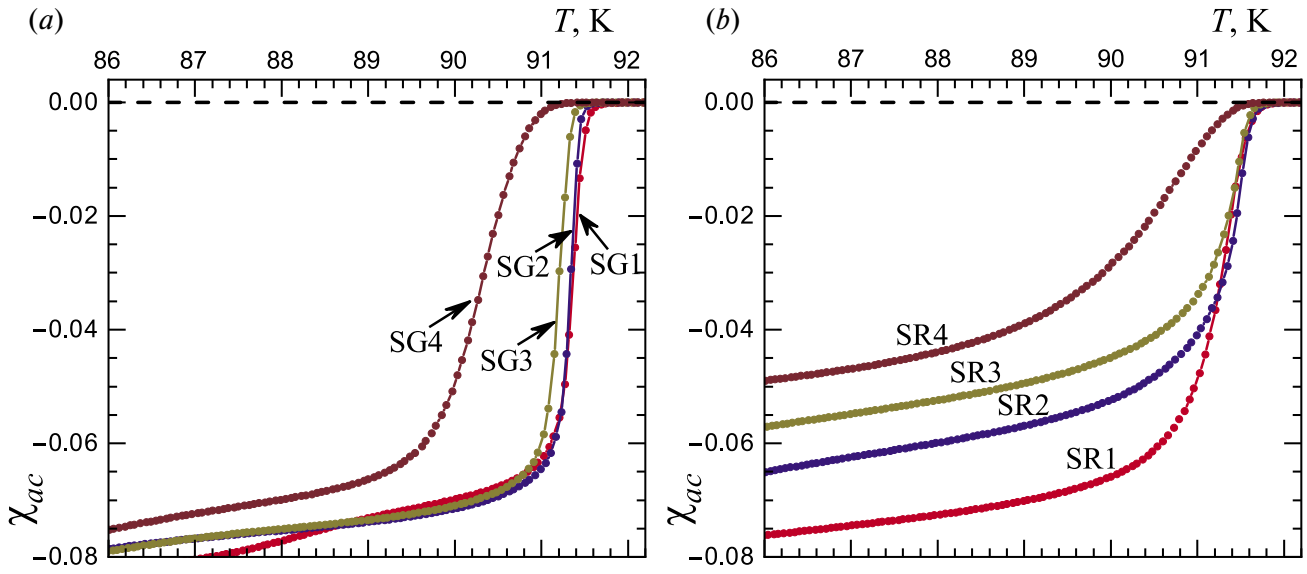

Fig. 4. Temperature dependencies of low-frequency magnetic susceptibility (amplitude of alternating magnetic field 3Oe) for HTSC samples $Y_{1-x}Fe_xBa_2Cu_3O_y$, synthesized using sol-gel process (*a*), solid-state method (*b*). Sample designations are shown near the curves

is also a noticeable transition broadening, indicating increasing structural inhomogeneity. Another result is the decrease in the effective screened volume of crystallites with increasing x in the solid-state synthesis method, which Fig. 4*b*. Analysis of equilibrium magnetization curves in high fields for these samples, conducted in [24], showed that this result is not related to the decrease in superconducting phase volume but is a manifestation of increased magnetic anisotropy of crystallites. The effects of Fe HTSC YBaCuO doping on anisotropy were also observed in [25].

The difference in synthesis methods had a significant impact on magnetic properties in a strong constant magnetic field. In sol-gel samples, the magnetization hysteresis range significantly increased $\Delta M(H)$, and features related to non-monotonic behavior of field dependencies became more pronounced (see Fig. 5).

Using formula (1), field dependencies of intracrystalline critical current density J_c were calculated from magnetization hysteresis measurement data. Results in the temperature range

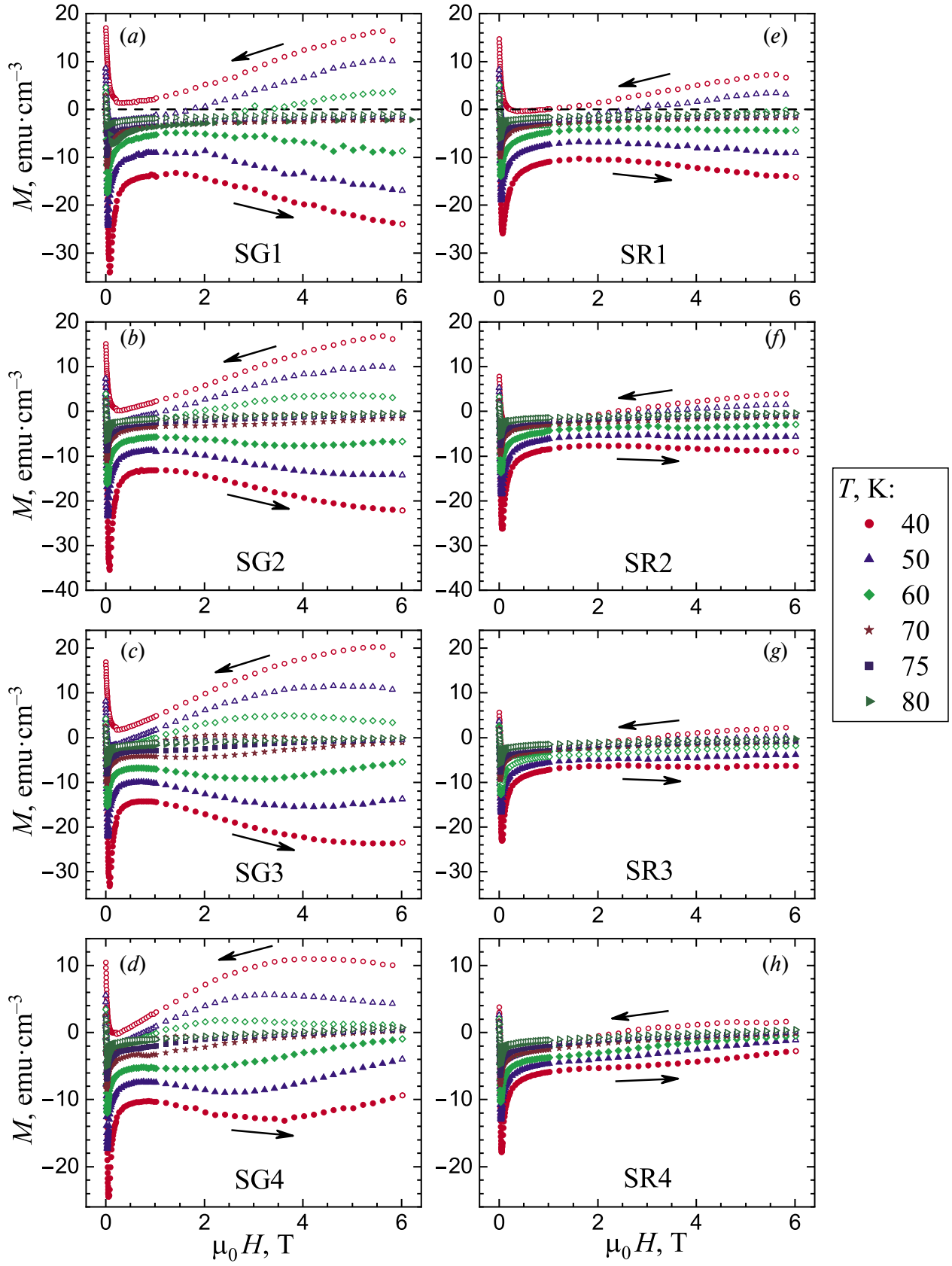

Fig. 5. Field dependencies of HTSC sample magnetization $Y_{1-x}Fe_xBa_2Cu_3O_y$ with different iron content x, synthesized using sol-gel process (*a, b, c, d*), solid-state method (*e, f, g, h*). Arrows indicate the direction of external field change

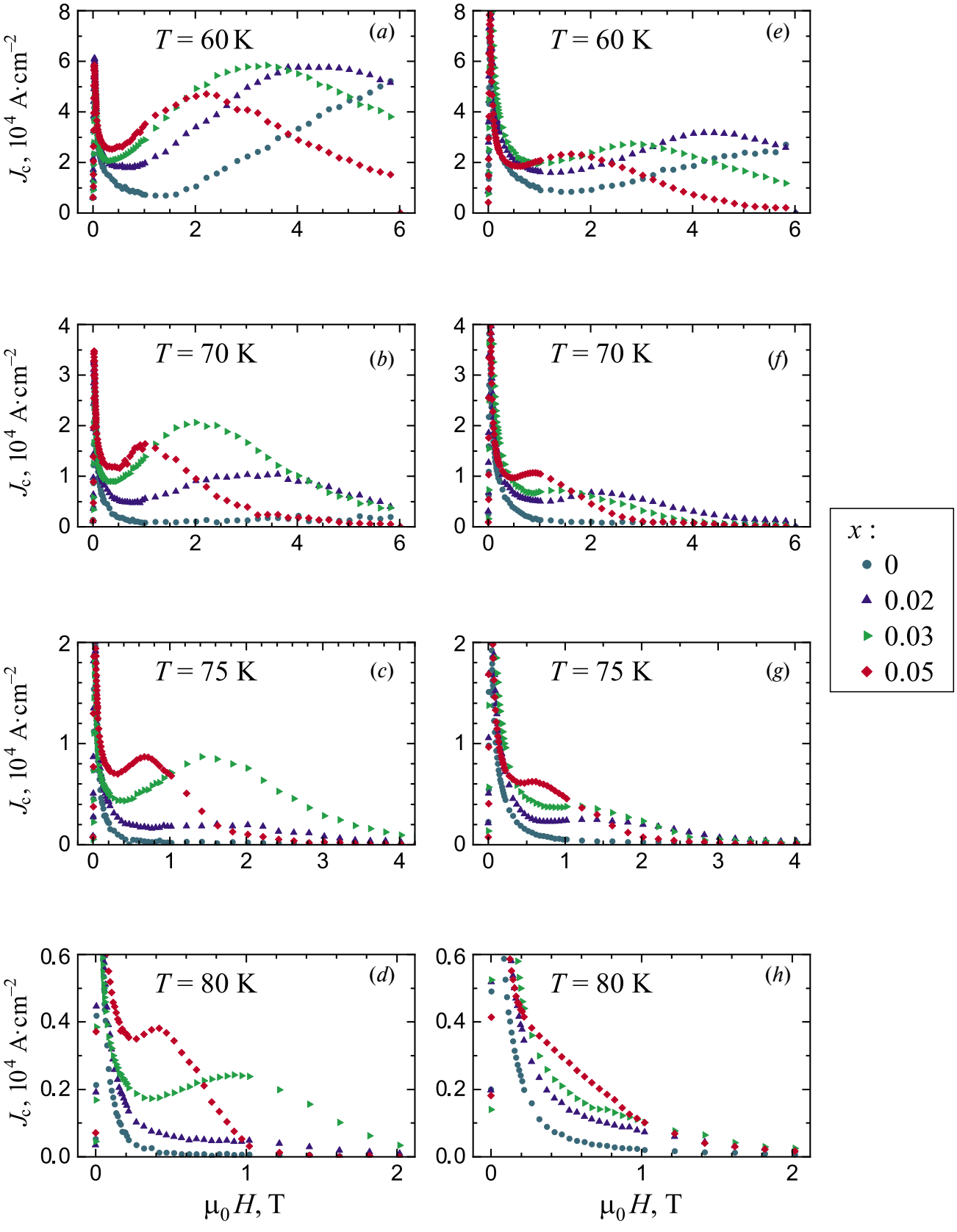

Fig. 6. Field dependencies of critical current density at temperatures $T = 60, 70, 75$ and 80 K for HTSC samples $Y_{1-x}Fe_xBa_2Cu_3O_y$ with different iron content x, synthesized using sol-gel process (*a, b, c, d*), solid-state method (*e, f, g, h*)

near liquid nitrogen boiling point, most important for practical applications, are shown in Fig. 6.

It is evident that pinning centers created by impurity iron significantly increase J_c compared to iron-free samples with both synthesis methods. The difference in synthesis method and, consequently, in the degree of spatial ordering of substitution atoms, manifested in higher values of J_c, as well as in a more pronounced second maximum on the curves $J_c(H)$ ("peak effect") in sol-gel samples. It should be noted that the peak effect also occurs with substitutions in copper and barium sublattices YBaCuO [10, 11, 13], however, in the system under consideration, the increase in J_c with the same degree of iron doping is approximately five times greater. According to existing concepts, the peak effect is a consequence of the interaction between the vortex lattice and the pinning center system. The magnetic field H_p, where J_c reaches its maximum, corresponds to a phase transition in the vortex lattice [26]. In this case, increasing the efficiency of vortex interaction with point defects, both due to increased concentration and temperature rise, should lead to a shift in the value of H_p toward lower fields [27]. This exact effect is observed in the studied samples with different Fe content (Fig. 6).

It is important to note that even with weak doping (a few percent), unit cells with cation substitution cannot be considered isolated in terms of the formation of the superconducting state and pinning effects. Indeed, at $x = 0.03$ the average distance between such cells is $(V_{cell}/x)^{1/3} \approx 1.8$ nm, which turns out to be on the order of the coherence length. Thus, a nanoscale system of magnetic defects is formed, where the interaction of vortices has a collective nature and is sensitive to the degree of ordering of substitution cations.

CONCLUSIONS

Two series of HTSC $Y_{1-x}Fe_xBa_2Cu_3O_y$ ($0 \leqslant x \leqslant 0.05$) were synthesized, differing in the method of obtaining the initial batch and subsequent high-temperature annealing. In the first series, sol-gel technology was used at the initial stage, while in the second, a mixture of commercial reagents was used. The use of the sol-gel process allowed to reduce the number, temperature, and time of annealing and to produce samples with significantly better structural and physical characteristics. A complex of X-ray, electron microscopic, and magnetic studies was conducted, determining the influence of the synthesis method on sample properties. It was shown that the sol-gel process allowed to obtain high-density large-crystalline samples (density reaches 93% of X-ray density) with more uniform distribution of substitution atoms. As a result, the temperature interval of the transition to the superconducting state decreased, the magnitude of the magnetic field hysteresis of magnetization increased, and the effects of non-monotonic magnetization behavior became more pronounced.

The spatially uniform distribution of pinning centers created by substitution atoms in sol-gel samples is manifested in increased critical current density and more pronounced second maximum in the field H_p on the field dependencies of intracrystalline critical current. The dependence H_p on the doping level allows for the selection of optimal composition of HTSC materials based on YBaCuO to achieve maximum critical current under given physical conditions (temperature and magnetic field) of practical application.

ACKNOWLEDGMENTS

Measurements of magnetic properties at low temperatures and in strong magnetic fields were performed using the equipment of the Center for Collective Use of PMI IGIC RAS. Microphotographs were obtained using a scanning electron microscope at the Center for Collective Use of PMI IPCE RAS.

FUNDING

The work was carried out with the support of a subsidy from the Ministry of Science and Higher Education of Russia, allocated to FRC CP RAS for the implementation of the state assignment on the topic "New Generation Nanostructured Systems with Unique Functional Properties" (No. 122040500071-0).

REFERENCES

1. G.V. M. Kiruthika, K.V. Govindan Kutty, and U.V. Varadarju, Solid State Ionics **110,** 335 (1998).

2. A.V. Shlyakhtina, N.V. Lyskov, A.N. Shchegolikhin, S.A. Chernyak, A.V. Knotko, I.V. Kolbanev, and L.G. Shcherbakova, Ceram. Int. **46,** 17383 (2020).

3. E.D. Politova, G.M. Kaleva, A.V. Mosunov, S. Yu. Stefanovich, E.V. Klyukina, E. A. Bespalova, A.V. Lopatin, N.M. Metal'nikov, M.E. Saprykin, A.B. Loginov, I.V. Orazov, B.A. Loginov, Inorg. Mater. **58,** 1328 (2022).

4. J. Ma, K. Chen, C. Li, X. Zhang, and L. An, Ceram. Int. **47,** 24348 (2021).

5. J. Zhang , S. Liu, Z. Tian, Y. Zhang, and Z. Shi, Materials **16,** 2214 (2023).

6. J. Mrázek, S. Kamrádková, J. Buršík, R. Skála, I. Bartoň, P. Varák, Y. Baravets, and O. Podrazkỳ, J. Sol-Gel Sci. Technol. **107,** 320 (2023).

7. B. Keimer, S.A. Kivelson, M.R. Norman, S. Uchida, and J. Zaanen, Nature **518,** 179 (2015).

8. L.G. Mamsurova, K.S. Pigalskiy, N.G. Trusevich, A.A. Vishnev, M.A. Rogova, S. Yu. Gavrilkin, A. Yu. Tsvetkov, JETP Letters **102,** 662 (2015).

9. J. Shimoyama, Y. Tazaki, Y. Ishii, T. Nakashima, S. Horii, and K. Kishio, J. of Phys.: Conf. Series **43,** 235 (2006).

10. Y. Ishii, J. Shimoyama, Y. Tazaki, T. Nakashima, S. Horii, and K. Kishio, Appl. Phys. Lett. **89,** 202514 (2006).

11. K. Rogacki, B. Dabrowski, and O. Chmaissem, Phys. Rev. B **73,** 224518 (2006).

12. A. Los, B. Dabrowski, and K. Rogacki, Cur. Appl. Phys. **27,** 1 (2021).

13. R.F. Lopes, V. N. Vieira, F. T. Dias, P. Pureur, J. Schaf, M.L. Hneda, and J.J. Roa, IEEE Trans.: Appl. Supercond. **26,** 8002004 (2016).

14. F. Minghu, C. Meng, J. Zhengkuan, and Z. Qirui, Jpn. J. Appl. Phys. **33,** 3892 (1994).

15. D.M. Gokhfeld, D.A. Balaev, I.S. Yakimov, M.I. Petrov, and S.V. Semenov, Ceram. Inter. **43,** 9985 (2017).

16. K.S. Pigalskiy, A.A. Vishnev, N.N. Efimov, A.V. Shabatin, and L.I. Trakhtenberg, Curr. Appl. Phys. **41,** 116 (2022).

17. M. Kakihana, J. Sol-Gel Sci. Technol. **6,** 7 (1996).

18. R. S. Liu, W. N. Wang, C.T. Chang, and P.T. Wu, Jpn. J. Appl. Phys. **28,** L2155 (1989).

19. E. Blinov, V.G. Fleisher, H. Huhtinen, R. Laiho, E. Lähderanta, P. Paturi, Yu. P. Stepanov, and L. Vlasenko, Supercond. Sci. Technol. **10,** 818 (1997).

20. J. Raittila, H. Huhtinen, P. Paturi, and Yu. P. Stepanov, Physica C **371,** 90 (2002).

21. L. G. Mamsurova, N. G. Trusevich, A.A. Vishnev, K.S. Pigalskiy, L.I. Trakhtenberg, Russ. J. Phys. Chem. B **14,** 986 (2020).

22. J.R. Clem and V.G. Kogan, Jap. J. Appl. Phys. **26,** 1161 (1987).

23. A.M. Balagurov, L. G. Mamsurova, I.A. Bobrikov, To Thanh Loan, V. Yu. Pomyakushin, K.S. Pigalskiy, N. G. Trusevich, A. A. Vishnev, JETP **114,** 1001 (2012).

24. K. S. Pigalskiy, N. N. Efimov, P. N. Vasilyev, A. A. Vishnev, and L.I. Trakhtenberg, Physica C **612,** 1354318 (2023).

25. T. Ugawa, S. Horii, T. Maeda, M. Haruta, and J. Shimoyama, Physica C **494,** 41 (2013).

26. Y. Paltiel, E. Zeldov, Y. N. Myasoedov, H. Shtrikman, S. Brattacharya, M.J. Higgins, Z.L. Xiao, E.Y. Andrei, P.L. Gammel, and D.J. Bishop, Nature **403,** 398 (2000).

27. G.P. Mikitik and E.H. Brandt, Phys. Rev.B **64,** 184514 (2001).